China Ocean Eng., 2019, Vol. 33, No. 5, P. 522–536
DOI: 10.1007/s13344-019-0050-4, ISSN 0890-5487
http://www.chinaoceanengin.cn/ E-mail: coe@nhri.cn

Numerical and Experimental Study of Blockage Effect Correction Method in Towing Tank

GUO Chun-yu[a], XU Pei[a], WANG Chao[a, *], KAN Zi[b]

[a]College of Shipbuilding Engineering, Harbin Engineering University, Harbin 150001, China

[b]Scool of Aeronautic Science and Engineering, Beihang University, Beijing 100191, China

Received May 3, 2018; revised March 11, 2019; accepted April 12, 2019

©2019 Chinese Ocean Engineering Society and Springer-Verlag GmbH Germany, part of Springer Nature

Abstract

When a ship model test is performed in a tank, particularly when the tank is small and the ship model is relatively large, the blockage effect will inevitably occur. With increased ship model scale and speed, the blockage effect becomes more obvious and must be corrected. In this study, the KRISO 3600 TEU Container Ship (KCS) is taken as a model and computational fluid dynamics techniques and ship resistance tests are applied to explore the mechanism and correction method of the blockage effect. By considering the degrees of freedom of the sinkage and trim, the resistance of the ship model is calculated in the infinite domain and for blockage ratios of 1.5%, 1.8%, 2.2%, and 3.0%. Through analysis of the free surface, pressure distribution, and flow field around the ship model, the action law of the blockage effect is studied. The Scott formula and mean flow correction formula based on the average cross sectional area are recommended as the main correction methods, and these formulas are improved using a factor for the return flow velocity correction based on comparison of the modified results given by different formulas. This modification method is verified by resistance test data obtained from three ship models with different scale ratios.

Key words: blockage effect, ship model resistance, blockage ratio, KCS ship, CFD

Citation: Guo, C. Y., Xu, P., Wang, C., Kan, Z., 2019. Numerical and experimental study of blockage effect correction method in towing tank. China Ocean Eng., 33(5): 522–536, doi: 10.1007/s13344-019-0050-4

1 Introduction

The tank boundary effect has been drawing attention since ship model tests in towing tanks were first conducted. The blockage effect is the main component of the tank boundary effect. With large-scale, high-speed development of ships, as well as acquisition of higher-accuracy test values and flow fields that match the real-world conditions, the sizes and test velocities of ship models have increased correspondingly, and the influence of the blockage effect has become more pronounced. Therefore, it is of practical significance to explore the law governing the blockage effect and to propose reasonable correction methods.

For a ship model test conducted in a tank, the obtained resistance value is larger than that obtained in the infinite domain at the same velocity, because of the influence of the boundary effect of the tank. Tank boundary effects can be divided into the blockage, shallow water, and sidewall effects. Shallow water and sidewall effects are less significant in conventional tanks (excluding shallow tanks), because of the velocity limits. Thus, the boundary effect of the tank is mainly related to the blockage effect (Xie et al., 1978). At the 13th International Towing Tank Conference (ITTC), Gross and Watanabe (1972) provided modified formulas for the blockage effect. Later, Xie et al. (1978) noted that, for a tank with a normal scale ratio λ (again excluding a shallow tank), the influence of the tank width on the resistance exceeds that of the tank depth, and the correction formula must be selected with consideration of the impact of the tank width-to-depth ratio. At present, increased numbers of researchers are studying the blockage effect in wind and water tunnels. Previously, William and Pope (1984) proposed a test to be performed in a low-speed wind tunnel, in which the blockage effect can be neglected when the blockage ratio m is smaller than 1.0%. Recently, Zaghi et al. (2016) have further verified the use of the Reynolds averaging method to study the possibility of blockage effects in wind tunnel tests, reporting good agreement between simulation and test results.

The blockage effect occurring in a ship model towing tank is similar to the principles applicable to a restricted channel; thus, research attention has been focused on the hydrodynamic performance of ships in restricted channels.

Foundation item: This research was financially supported by the National Natural Science Foundation of China (Grant No. 51679052), the Natural Science Foundation of Heilongjiang Province of China (Grant No. E2018026) and the Defense Industrial Technology Development Program (Grant No. JCKY 2016604B001).

*Corresponding author. E-mail: wangchao806@hrbeu.edu.cn

Various authors (Beck, 1981; Millward, 1996; Jachowski, 2008; Zhou et al., 2013) have used computational fluid dynamics (CFD) techniques to study the influence of the water depth, width, and ship velocity on the hull squat and waveform. The CFD results were compared with empirically obtained data. Theoretical methods have also been developed to determine the squat and trim of ships sailing in restricted water (Schijf, 1949; Gourlay, 2008; Alderf et al., 2010). Previously, Ma et al. (2013) used CFD techniques to study the influence of the sidewall effect in a restricted channel, and the force and moment of the hull were calculated for different offshore distances in shallow water. In addition, Zou and Larsson (2013a, 2013b) studied the possibility of using different CFD methods to calculate the sidewall effect in shallow water. The Korea Research Institute of Ships and Ocean Engineering (KRISO) Very Large Crude-oil Carrier (KVLCC2) ship model was used and the force and squat changes on the hull were calculated at different water depths and offshore distances. Those researchers' results revealed that the Reynolds-averaged Navier–Stokes method has good computational accuracy, but the improved accuracy can be obtained with the shear stress transport (SST) k–ω turbulence model. Finally, Zhang et al. (2015) studied the hydrodynamic pressure field in the restricted water domain by calculating the hydrodynamic pressure and comparing the results with experimentally obtained values. Hence, it was proposed that the effect of the watercourse can be neglected when the width of the rectangular channel is three times larger than the ship length.

However, in comparison with theory-based researches, there are few experiment-based studies of the blockage effect in a towing tank. Previously, Zhou (2002) and Wu (2007) analyzed the blockage effect when investigating the uncertainties of ship model resistance tests; however, they used the ITTC formula to modify the speed and did not improve upon the revised formula. In addition, Lataire et al. (2012) studied the effects of the widths and depths of different tanks on the squat of the KVLCC2 ship model in a shallow-water towing tank, and proposed a mathematical model to solve the squat change of ship.

In this study, the SST k–ω turbulence model is used to analyze the blockage effect mechanism and correction method for the KCS. The volume of fluid (VOF) method is used to capture the free surface of the ship in order to calculate the hull heave, trim, and resistance for different widths and depths, to explore the law governing the blockage effect. In addition, three different λ values for the KCS model are used in a ship model resistance test performed in the Harbin Engineering University towing tank, to propose the blockage effect correction method.

2 Numerical model

2.1 Control equation

The motion of an incompressible Newtonian fluid satisfies the continuity equation and momentum conservation equation (Wilcox, 1998):

$$\frac{\partial \rho}{\partial t}+\frac{\partial(\rho u_i)}{\partial x_i}=0; \tag{1}$$

$$\frac{\partial(\rho u_i)}{\partial t}+\frac{\partial(\rho u_i u_j)}{\partial x_j}=-\frac{\partial p}{\partial x_j}+\frac{\partial}{\partial x_j}\left(\mu\frac{\partial u_i}{\partial x_j}-\rho\overline{u_i' u_j'}\right)+S_j, \tag{2}$$

where u_i and u_j (i, j = 1, 2, 3) are the time-averaged velocity components; p is the time-averaged pressure; μ is the dynamic viscous coefficient; ρ is the fluid density; $\rho\overline{u_i' u_j'}$ is the Reynolds stress term; and S_j is the generalized source term of the momentum equation.

2.2 Turbulence model and treatment of the free surface

The SST k–ω model is used in the turbulence model (Menter, 1994). The former model combines the advantages of the k–ω model and k–ε model and has good advantages as regards calculation of a viscous flow field. The basic principle of the VOF method is to determine the free surface by investigating the volume ratio function of the fluid and grid in the mesh cell, and to track the changes in the fluid rather than the movement of particles on the free surface (Hirt and Nichols, 1981; Wang et al., 2015). This method can trace the complex free surface phenomenon. In addition, the calculation requires less memory than other techniques and is easy to implement and expand to three dimensions. The changes in the free surface are captured by the VOF method.

3 Computational model and grid

3.1 Calculation model and calculation conditions

In this study, the KCS model is taken as the research object; the geometric model is shown in Fig. 1 and the main parameters of the ship model are listed in Table 1.

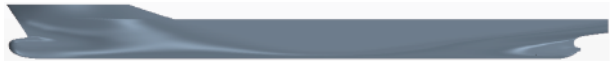

Fig. 1. Geometric model of KCS.

In this study, the ship model resistance, heave, and trim were calculated for five operating conditions, for which the blockage ratio (defined as $m = (B\times T)/(b\times h)$, where B, T, b, and h are the molded ship breadth, ship draft, tank breadth, and tank depth, respectively) was set to 1.5%, 1.8%, 2.2%, 3.0%, and 0.1% (infinite domain) (Lataire et al., 2012). The Froude numbers Fr were 0.217, 0.227, 0.238, 0.249, 0.260, 0.271, and 0.282. Table 2 and Fig. 2 present the descriptions of the operating conditions for the calculation.

3.2 Boundary condition setting and grid partition

As the result of the blockage effect, the boundary conditions differ between the infinite and finite domains.

As shown in Fig. 3, in the infinite domain, the inlet, top,

Table 1 Main parameters of ship model

Parameter	Value
Length between perpendiculars L_{pp} (m)	7.2787
Molded breadth B (m)	1.019
Draft T (m)	0.3418
Wetted surface area S_W (m^2)	9.5443
Displacement volume of the model ∇ (m^3)	1.649
Block coefficient C_B	0.651
Design speed (m/s)	2.196
Scale ratio λ	31.599

Table 2 Calculation conditions

Project	Tank breadth b (m)	Tank depth h (m)	Molded breadth B (m)	Draft T (m)	Blockage ratio m
1	∞	∞	1.0194	0.3418	0.1%
2	7.0	3.50	1.0194	0.3418	1.5%
3	6.3	3.15	1.0194	0.3418	1.8%
4	5.6	2.80	1.0194	0.3418	2.2%
5	4.9	2.45	1.0194	0.3418	3.0%

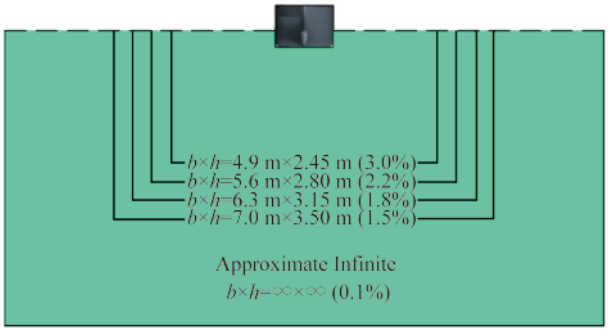

Fig. 2. KCS calculation conditions.

side, and bottom were set as the velocity inlet, and the outlet was set to the pressure outlet. In the finite domain, the effect of the sidewall and bottom must be considered. Therefore, the sidewall and bottom in the finite domain were set as walls, unlike the infinite domain case.

Before the calculation, the grid independence was verified, and the grid factor interference was eliminated by comparing calculated values of the three different sets of sparsity levels with experimentally obtained values (Yao et al., 2013). In this study, the $y+$ value range was controlled from 30 to 60, which shows that the mesh division of the boundary layer was reasonable. The grid partitions of the computational model are shown in Fig. 4.

4 Numerical investigation of the blockage effect mechanism

The blockage effect has an impact on ship model resistance tests featuring a towing tank, as the tank size is limited. In the past, it was difficult to study the microscopic effects of the blockage effect because of the limitations of the experimental instruments and test methods. Generally, the influence of the blockage effect on the total resistance of the ship model only was considered in previous studies. However, an application of CFD technology to this field has made acquisition of microscopic information such as details of the flow field more convenient, allowing more in-depth study of the blockage effect. In this section, the KCS is taken as an example and the blockage effect is studied with regard to the hull pressure, free surface wave height, wave profile, and flow field around the ship (Deng et al., 2014). Except for the special instructions, the speed of the KCS vessel in this section was the design speed, i.e., 2.196 m/s, for which the corresponding Fr is 0.26, and the design speed of the prototype is 12.347 m/s (i.e., 24.0 knots).

4.1 Analysis of the blockage effect influence on the free surface

To study the microscopic effects of the blockage effect, the reliability of the free surface calculation was first verified. Fig. 5 presents a comparison of the free surface extracted from the CFD calculation and the free surface obtained from previous experimental measurements by Kim et al. (2001). The y/L_{pp} values of 0.074, 0.151, and 0.302 indicated by the dashed lines in the figure correspond to three characteristic cross sections. As can be seen from Fig. 5, the calculated data are close to the experimental ones as regards the quantitative wave height distribution, and the dis-

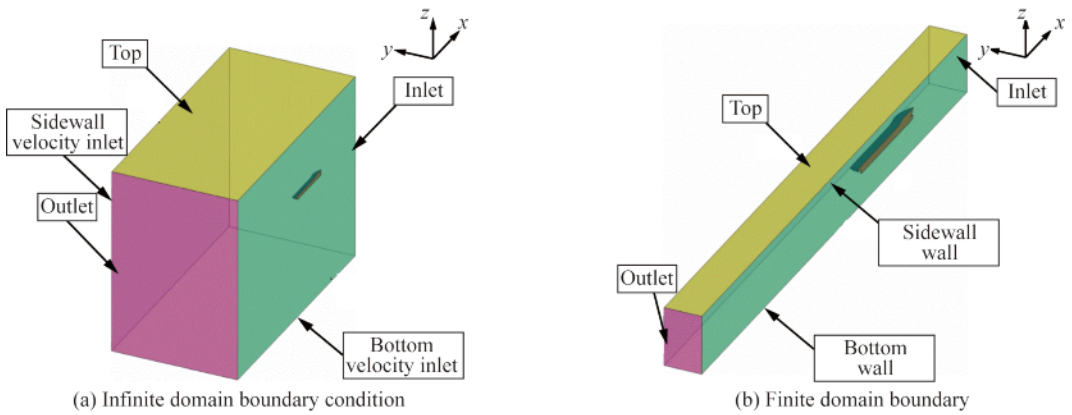

Fig. 3. Infinite domain and finite domain boundary condition settings.

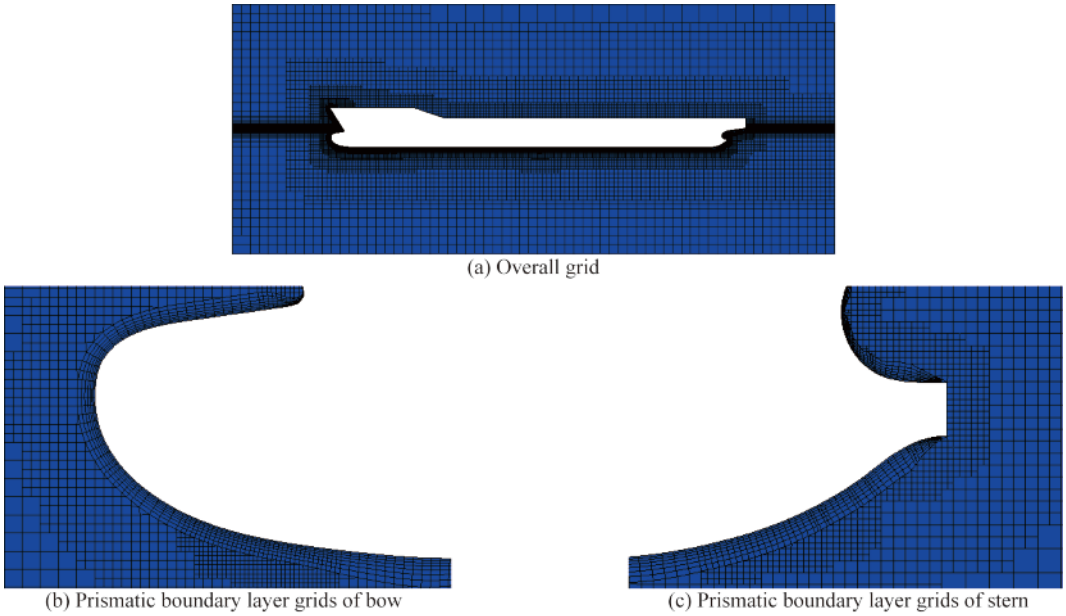

Fig. 4. Grid distribution.

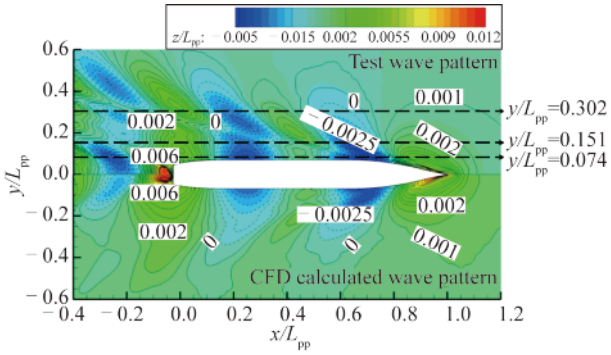

Fig. 5. Comparison of CFD calculated and experimentally measured (Kim et al., 2001) free surface wave patterns for KCS.

tribution positions of the peaks and troughs are also very close. In the range of the target observation area y/L_{pp} = ±0.302 in particular, the calculated and experimentally obtained wave profile distributions are similar; thus, the free surface calculation is reliable. Fig. 6 presents a comparison of the calculated and experimentally obtained hull wave profiles (Kim et al., 2001). Again, the calculated CFD values are quite close to the experimental ones, which further proves the reliability of the calculated results.

Figs. 7 and 8 show comparisons of the free surface wave-making obtained at different m. In detail, Fig. 7 presents a comparison of the free surface wave-making obtained for the infinite domain and a finite domain for which m was 1.5%. Fig. 8 gives a comparison of the m = 3.0% domain and the infinite domain. As can be seen from these figures, the wave pattern does not vary largely with an increase in m. Instead, a higher m only causes the wave patterns at the bow and stern of the ship to become larger and slightly confused. Comparison of the contour values reveals that, with increased m, the value at a given position near the hull undergoes a significant change. However, there are no significant changes in the waves behind the stern.

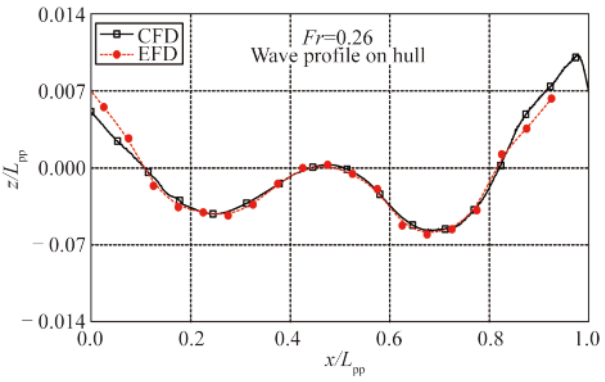

Fig. 6. CFD calculated and experimentally measured (EFD) (Kim et al., 2001) wave profile contrasts on hull.

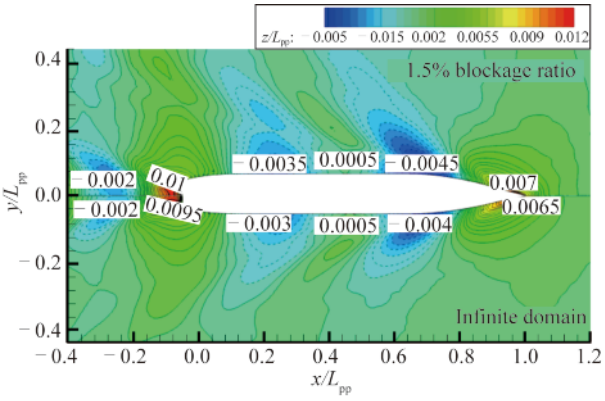

Fig. 7. Comparison of KCS free surface wave patterns for m = 1.5% and infinite domain.

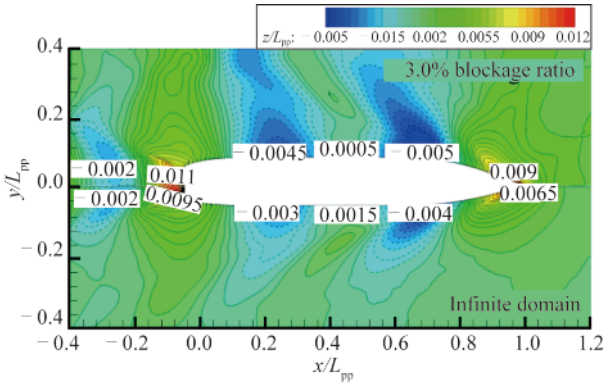

Fig. 8. Comparison of KCS free surface wave patterns for m = 3.0% and infinite domain.

To quantitatively study the influence of the blockage effect on the free surface wave-making, the wave heights of three characteristic sections with y/L_{pp} = 0.074, 0.151, and 0.302 were compared under different m values, as shown in Figs. 9–11. It can be seen from these figures that, in the y/L_{pp} = 0.074 section and for m = 1.5% and 2.2%, the wave height changes very slightly. However, when m is equal to 3.0%, the wave height fluctuates dramatically. The same rule applies for y/L_{pp} = 0.151. For y/L_{pp} = 0.302, the amplitude variation decreases with increasing distance from the hull, with the largest amplitude still being obtained for m = 3.0%. Obviously, the blockage effect affects the wave height around the hull and, as m increases, the free surface wave amplitude also increases.

To more clearly compare the changes caused by the blockage effect on the free surface wave-making around the hull, a comparison chart of the hull wave height is presented in Fig. 12. Hence, it is obvious that the amplitude of the hull wave is at a maximum when m is at a maximum. From the energy perspective, it is the blockage effect that increases the wave amplitude of the hull and its surroundings, and this aspect of the energy loss is finally reflected by an increase in the total resistance of the ship model.

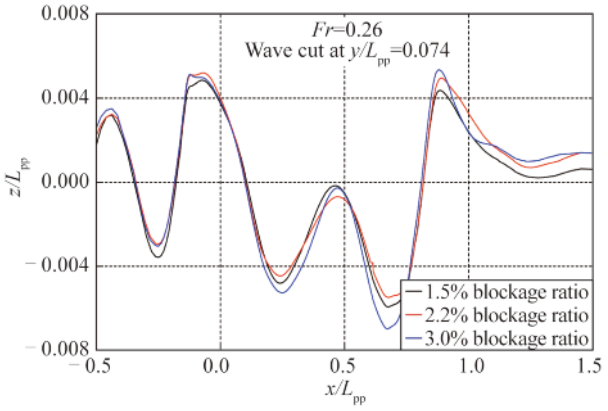

Fig. 9. Comparison of wave heights at different blockage ratios for y/L_{pp} = 0.074.

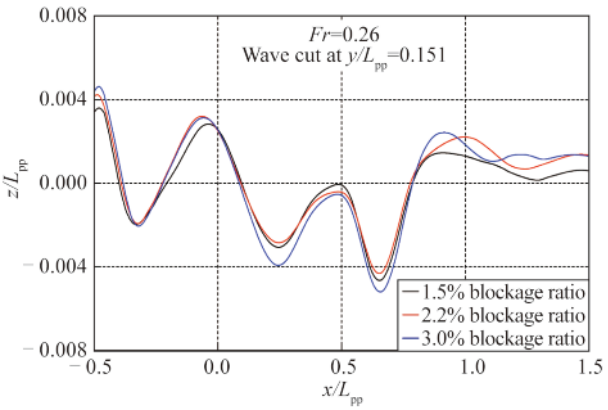

Fig. 10. Comparison of wave heights at different blockage ratios for y/L_{pp} = 0.151.

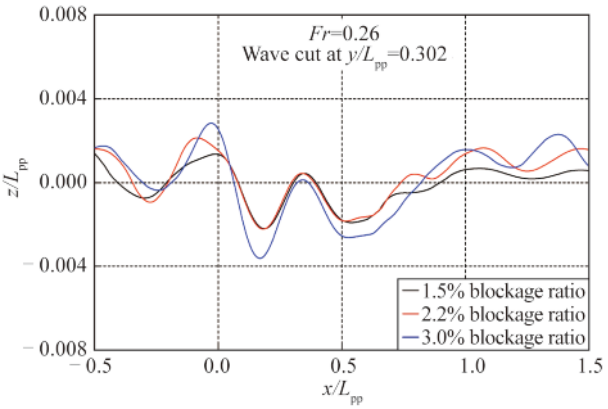

Fig. 11. Comparison of wave heights at different blockage ratios for y/L_{pp} = 0.302.

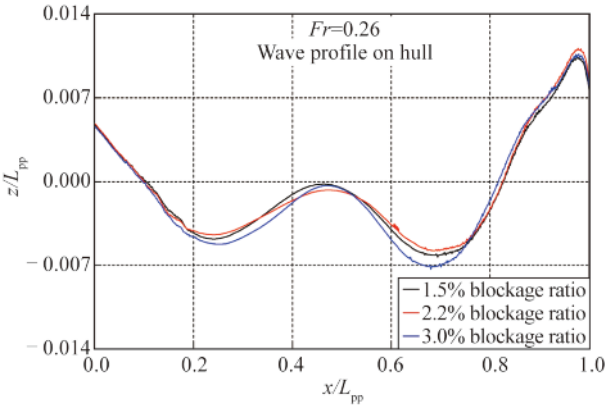

Fig. 12. Comparison of wave profiles on hull obtained for different blockage ratios.

4.2 Analysis of the influence of the blockage effect on the hull pressure

When a ship model resistance test is performed in a towing tank, the movement of the flow around the ship model is limited by the presence of the tank bottom and wall, so that the flow velocity around the ship model is higher than that for the infinite domain. According to the Bernoulli equation,

a change in flow velocity changes the hull pressure. In this study, the hydrostatic pressure was subtracted from the calculated total pressure to obtain the pressure, and the pressure coefficient was defined as $C_p = P/(1/2\rho v^2)$. Figs. 13 and 14 show the distributions of the hull pressure coefficients obtained at different m. In detail, Figs. 13 and 14 show the pressure distributions at the bottom of the ship and on the bow and stern of the ship, respectively, for m = 3.0% and the infinite domain. From Fig. 13, it is obvious that the pressure at the bow of the ship's bottom is larger than that at the stern of the ship's bottom, such that a viscous resistance is produced. The numerical results presented in Fig. 13 indicate that larger resistance is obtained for m = 3.0% than that for the infinite domain case. Comparison of the results for these two cases presented in Fig. 13 reveals that the blockage effect yields a bottom flow velocity in the middle and stern of the ship that is slightly larger than that in the infinite domain, resulting in a decrease in pressure. As the bottom of the ship's bow corresponds to a bulbous nose, the wetted surface is small and the pressure changes are not obvious.

As can be seen from the pressure distribution on the ship's side shown in Fig. 14, the low-pressure area is distributed on both sides of the bulbous bow, and the pressure in this area at m = 3.0% is lower than that in the infinite domain. This is because of the blockage effect at the bow of the ship. As a result, the flow near the bow is squeezed to both sides of the ship hull, yielding a larger return flow velocity, which reduces the pressure at the bow. The numerically calculated pressure distribution at the stern indicates that the pressure change is less obvious than that at the bow, but the pressure contour distribution is relatively confused at m = 3.0%.

To more clearly observe the changes in the pressure at

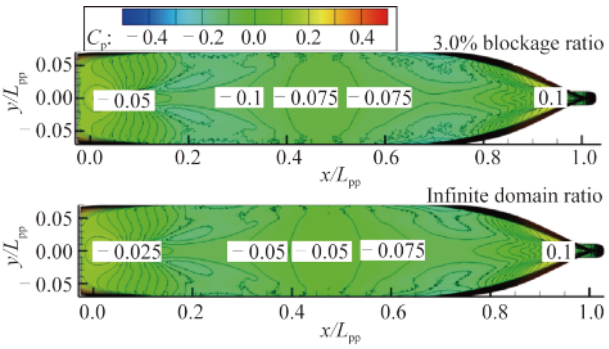

Fig. 13. Comparison of pressure distributions on ship bottom for m = 3.0% and infinite domain.

the stern, the Q-criterion vortex structure distribution of the KCS hull was extracted, and the stern bilge vortex was primarily observed (Hunt et al., 1988). The calculation formula for Q is as follows:

$$Q = -\frac{1}{2}\left[\left(\frac{\partial u}{\partial x}\right)^2 + \left(\frac{\partial v}{\partial y}\right)^2 + \left(\frac{\partial w}{\partial z}\right)^2\right] - \left(\frac{\partial u}{\partial y}\frac{\partial v}{\partial x} + \frac{\partial u}{\partial z}\frac{\partial w}{\partial x} + \frac{\partial v}{\partial z}\frac{\partial w}{\partial y}\right). \quad (3)$$

Fig. 15 shows the vortex structure distributions with Q-criterion = 20 obtained for m = 3.0% and the infinite domain. The areas shown in the figures correspond to the stern bilge vortices. In Fig. 15, because of the presence of the blockage effect, the stern bilge vortex structures are less smooth than those in the infinite domain, which means that the blockage induces chaotic behavior in the flow field behind the stern. In addition, in Fig. 15, the stern bilge vortex becomes very small in the infinite domain, whereas that under the blockage condition remains obvious. The blockage emphasizes the whirlpool after the stern, which further de-

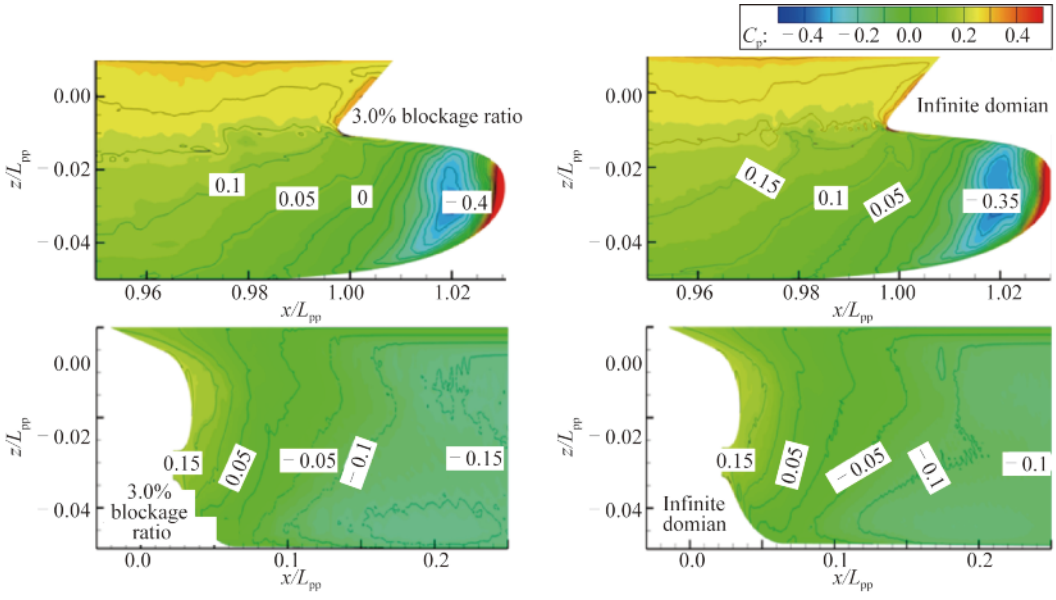

Fig. 14. Comparison of pressure distributions at ship bow and stern for m = 3.0% and infinite domain.

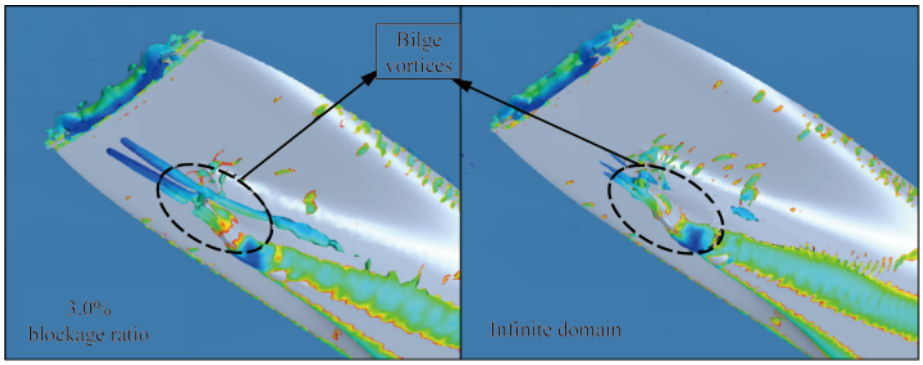

Fig. 15. Vortex structure distributions for Q-criterion = 20 at bottom and stern of KCS for m = 3.0% and infinite domain.

creases the stern pressure, resulting in a larger increase in the viscous resistance.

4.3 Hull squat change caused by blockage effect

In this study, the two degrees of freedom of the sinkage and trim were considered in the calculation. Fig. 16 shows the variations of the hull sinkage and trim with the ship model speed under different m values. The running trim was defined as positive when the bow moved downward, and the dynamic sinkage was defined as positive when the hull moved upward.

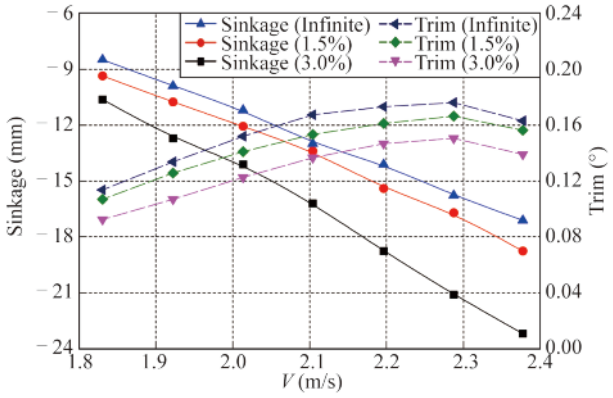

Fig. 16. Sinkage and trim curves as functions of velocity.

From Fig. 16, with the increase of speed, the ship hull sinks during traveling, which is accompanied by the phenomenon of trimming by the bow. The degree of sinking of the ship's hull increases with the increasing m, and the degree of trimming by the bow of the hull decreases. In accordance with the above analysis, there are more vortices in the stern, which causes the stern pressure to decrease. Therefore, the increment of the return flow velocity in the stern of the ship is larger than that of the bow, and the stern sinks to a larger degree than the bow, which results in a slight decrease in the degree of trimming by the bow.

4.4 Variation of flow field around KCS model

In this subsection, the blockage effect is analyzed through comparison of the flow field distributions of the KCS for different m. First, the ship wake field calculated via CFD is compared with experimentally measured values (Guo et al., 2016b), as shown in Fig. 17. In this figure, the velocity contours of both sides are similar, indicating that the calculation results are accurate.

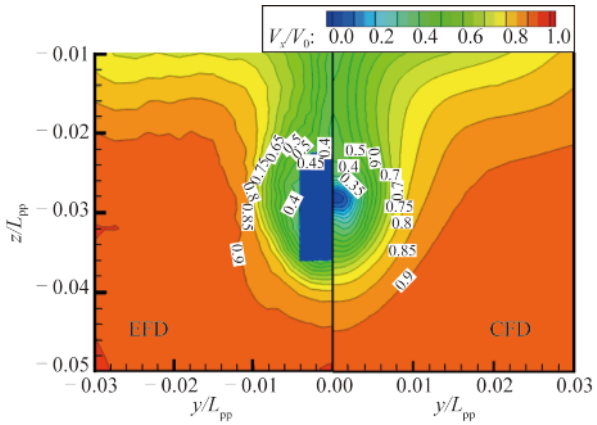

Fig. 17. Flow field distribution contrast diagram for KCS, CFD and EFD values (Guo et al., 2016b).

To more clearly show the influence of the blockage effect on the flow field around the hull, six cross-sections were selected for flow field information extraction, including five vertical sections (x/L_{pp} = 0.05, 0.15, 0.5, 0.9, and 1) and one horizontal section (z/T = 0.5). The specific positions are shown in Fig. 18.

Figs. 19–24 show the profile velocity distributions of the ship model at 2.196 m/s, for different cross-sections. The contour lines in the figures represent the dimensionless velocities in the x-axis direction, which is in accordance with the ship's forward direction. This is the main component of the flow field and the main cause of the changes in the ship model pressure. The arrows in the figures indicate the velocity components in the y and z directions. The arrow directions and lengths indicate the velocity direction and magnitude, respectively, which aid observation of the vortex structure and flow motion around the hull.

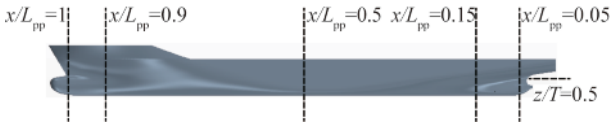

Fig. 18. Diagrammatic sketch of KCS ship profile with cross-section positions.

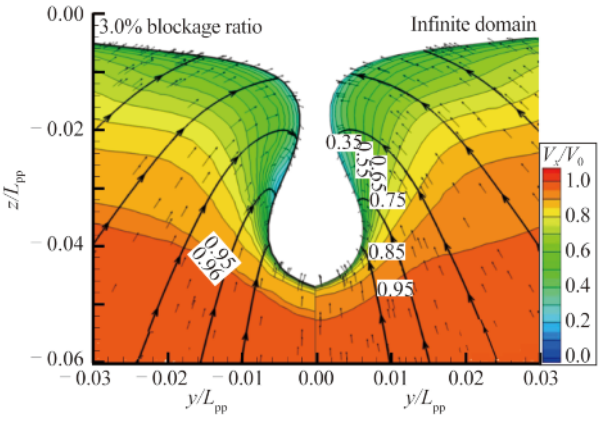

Fig. 19. Flow field distribution at x/L_{pp} = 0.05.

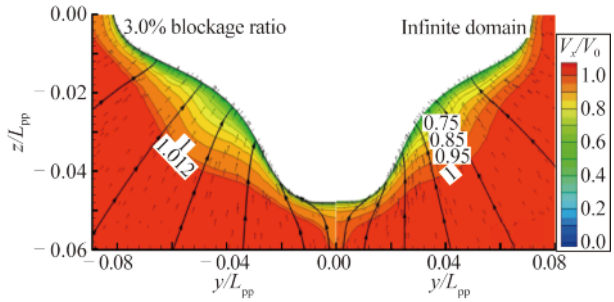

Fig. 20. Flow field distribution at x/L_{pp} = 0.15.

Figs. 19 and 20 show the flow field distribution of the hull at x/L_{pp} = 0.05 and 0.15, respectively. As shown in Fig. 19, a thicker boundary layer is found at x/L_{pp} = 0.05 than 0.15 (Fig. 20), which means that the flow discharge is more obvious. The most outlying value of the boundary layer shows that the blockage effect increases the speed by 1.05%; however, V_x/V_0 is always smaller than 1 at each position, which is in line with the theory of the ship's boundary layer. From the energy perspective, when the hull moves, it drives the flows in the boundary layers to move together. Under the influence of the blockage effect, the portion of the water driven by the hull has more kinetic energy, and this kinetic energy component is finally embodied in the form of ship model resistance. Note that the same distribution was observed for the flow field at x/L_{pp} = 0.15 (Fig. 20). However, under this blockage condition, the velocity is larger than V_0 and the boundary layer is thinner. Furthermore, the blockage effect causes an increase of 1.2% in the speed.

Fig. 21 shows the distribution of the flow field in the middle of the hull, where the boundary layer thickness decreases significantly. In addition, because the hull is wider

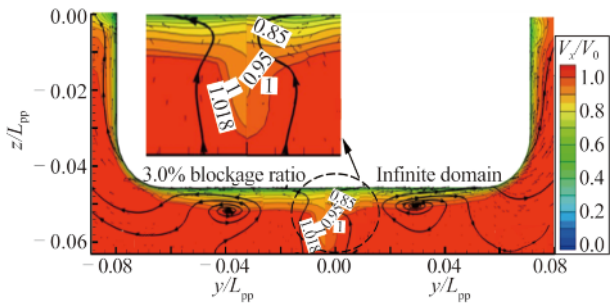

Fig. 21. Flow field distribution at x/L_{pp} = 0.5.

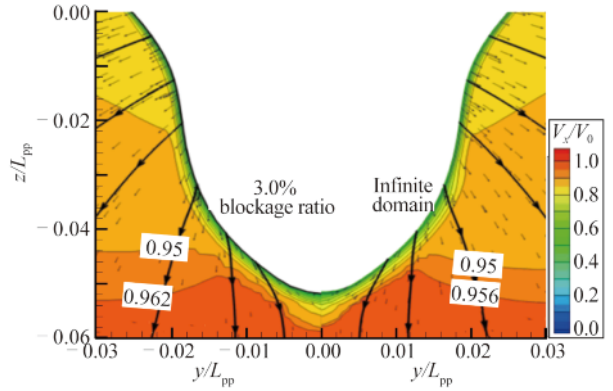

Fig. 22. Flow field distribution at x/L_{pp} = 0.9.

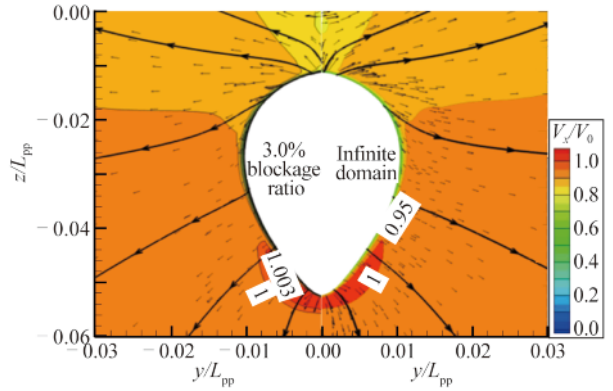

Fig. 23. Flow field distribution at x/L_{pp} = 1.

in the middle of the ship, the outward incoming flow at the bow creates swirls subjected to reverse pressure. It is obvious that, under the blockage condition, the whirlpool at the bottom of the ship has a wider range and the flow field in that location is more chaotic than that in the infinite domain. Observed from the outermost side of the boundary layer, the blockage effect increases the velocity of the flow around the hull by 1.8%.

Figs. 22 and 23 show the distributions of the flow field near the bow at different cross-sections. The boundary layer thickness at the bow decreases significantly. At x/L_{pp} = 0.9 (Fig. 22), the flow velocity is smaller than V_0. The streamlines in the figure flow downward and outward from the

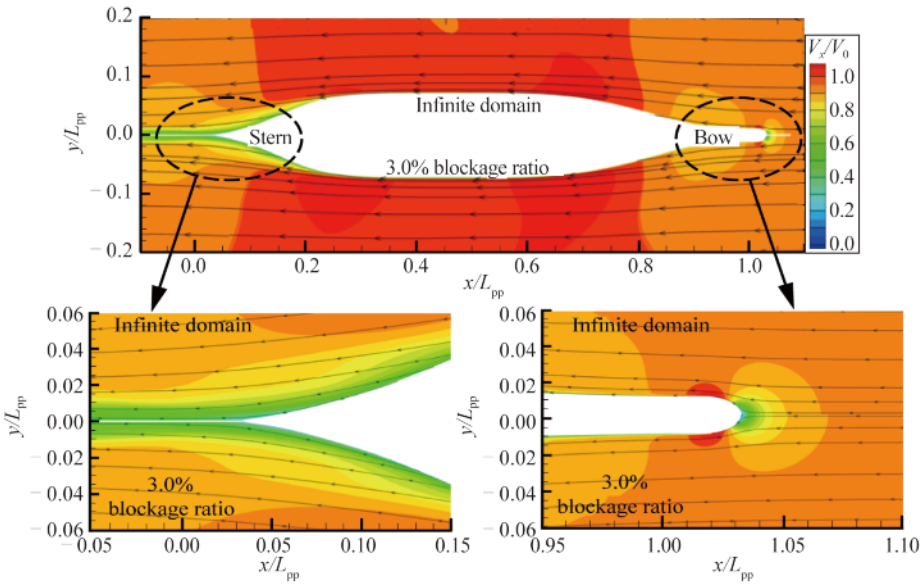

Fig. 24. Flow distribution at $z/L_{pp} = 0.5T$ section of the KCS.

hull, indicating that the flow is squeezed by the hull or congested in the bow, so that the blockage effect is also described as the congestion effect of the water at the bow. Here, the blockage effect increases the flow velocity by 0.6%. Fig. 23 shows that the minimum boundary layer thickness is obtained at $x/L_{pp} = 1.0$. Besides the small high-velocity zone at the bottom, the velocity of the flow is smaller than V_0. In addition, it can be seen that the flow velocity increases by 0.3% under the blockage condition.

Fig. 24 shows the flow field distribution at the horizontal section, at $z/L_{pp} = 0.5T$. An intuitive observation can be performed when the boundary layer is thicker from the bow to the stern. The blockage effect has no significant influence on the flow field distribution when the bow or stern is far from the boundary layer. Therefore, the flow field around the hull boundary layer merits considerable attention when studying the blockage effect mechanism.

5 Blockage effect correction method

5.1 Analysis of ship model resistance data

Fig. 25 shows the total resistance curves of the KCS model as functions of speed for different m. It is obvious that the blockage effect has a great influence on the resistance value; however, this influence varies with the value of m. At the same water depth Froude number Fr_h, the larger the value of m, the more significant the increase in the resistance value. The larger Fr_h, the more significant the blockage effect. Thus, as can be seen from Fig. 25, the influence of the blockage effect on the model resistance test is significant and correction of this effect is necessary.

5.2 Comparison of blockage effect corrections given by different formulas

Usually, m is the main parameter of the blockage effect correction and the required correction formula is selected according to m. The return flow velocity is calculated to correct the velocity-resistance curves shown above (Fig. 25).

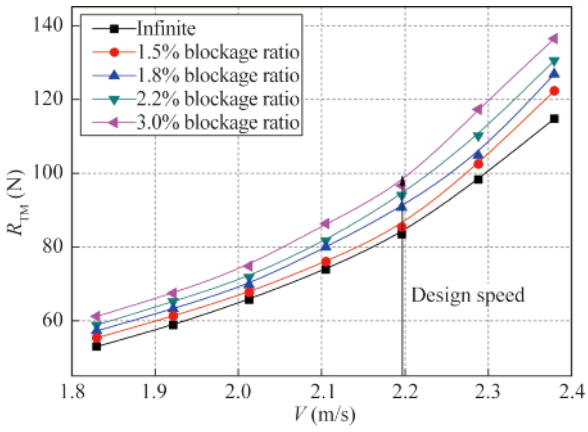

Fig. 25. Total resistance curves obtained for different m.

5.2.1 *Return flow velocity calculation*

At present, the most direct and simplest method of correcting the blockage effect is to correct the return flow velocity (Guo et al., 2016a). Formulas such as the Tamura simplified formula (Tamura, 1975), Scott formula (Scott, 1970), average flow m_1 formula, and average flow m_2 formula (Xie et al., 1978) (Eqs. (4)–(7), respectively) are widely used for return flow velocity calculation. In this study, the known resistance curves were corrected using each of these formulas to allow direct comparison of their correction effects.

$$\frac{\Delta v}{v} = 0.85 m_1 \left(\frac{L}{b}\right)^{\frac{3}{4}} \frac{1}{1 - Fr_h^2}; \tag{4}$$

$$\frac{\Delta v}{v} = \left(1.86 - 0.072 \times 10^{-6} Re\right) \cdot \nabla A^{-\frac{3}{2}} + BL^2 \left[2.4 \times (Fr_L - 0.22)^2\right] A^{-\frac{3}{2}}; \quad (5)$$

$$\frac{\Delta v}{v} = \frac{m_1}{1 - m_1 - Fr_h^2}; \quad (6)$$

$$\frac{\Delta v}{v} = \frac{m_2}{1 - m_2 - Fr_h^2}, \quad (7)$$

where Δv is the calculated return flow velocity; v represents the ship model velocity in the finite domain; Fr_h is the water depth Froude number, $Fr_h = v/\sqrt{gh}$; Re is the Reynolds number; A is the sectional area of the tank, $A = b \times h$; Fr_L is the ship length Froude number, $Fr_L = v/\sqrt{gL_{WL}}$; m_1 and m_2 are the blockage ratios, $m_1 = a_m/A = BTC_M/(b \times h)$, $m_2 = a/A = \nabla/L_{WL}/(b \times h)$; and the other parameters are defined previously.

5.2.2 *Comparison of correction effects*

To intuitively compare the correction effects of each formula for different m values, the velocity-resistance curves were modified using the return flow velocities calculated from the above formulas, i.e., Eqs. (4)–(7). Figs. 26–29 show the correction curves obtained when m was set to 1.5%, 1.8%, 2.2%, and 3.0%, respectively. In these figures, "Infinite", "Scott", "S-T", "m_1", and "m_2" indicate the resistance curve of the infinite domain and corrected curves obtained using the Scott formula, the Tamura simplified formula, and the m_1 and m_2 formulas, respectively. The X- and Y-axes indicate the ship model velocity and the total resistance of the ship model, respectively.

It can be seen from Fig. 26 that the four correction formulas all yield good results when m is 1.5%. The corrected resistance curve is almost coincident with the infinite domain resistance curve. However, the corrected curve is slightly above the infinite domain resistance curve in most areas; thus, the blockage effect corrections given by the four considered formulas are inadequate for this m. From Fig. 27, excluding the result for the average flow m_2 formula, the correction effects of the other formulas are still relatively good, and the sensitivity of each formula to the blockage effect in this state is beginning to become more inadequate. For m values of 2.2% and 3.0%, as shown in Figs. 28 and 29, respectively, the lack of sensitivity of the average flow m_2 formula is more obvious. In addition, when m is large, the Tamura simplified formula and Scott formula have better sensitivity, while the average flow m_1 formula yields a good correction effect when m is relatively small.

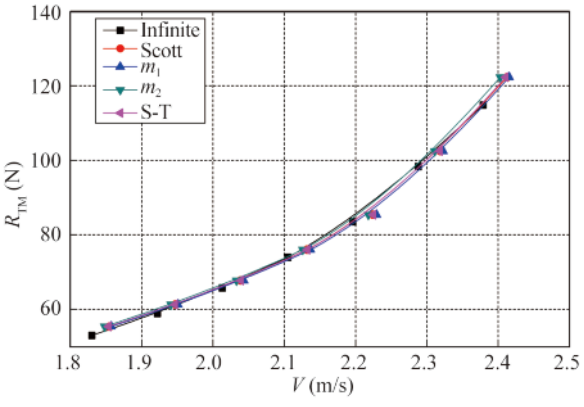

Fig. 26. Comparison of correction results for m = 1.5%.

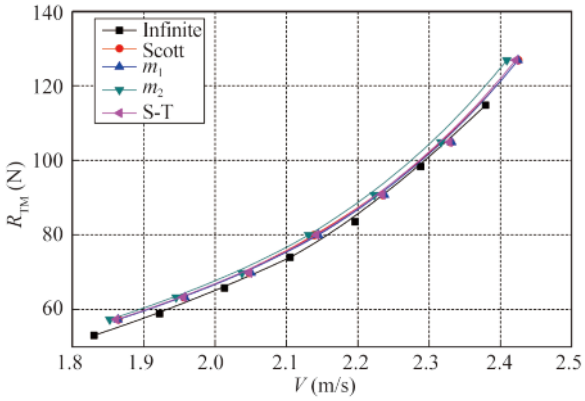

Fig. 27. Comparison of correction results for m = 1.8%.

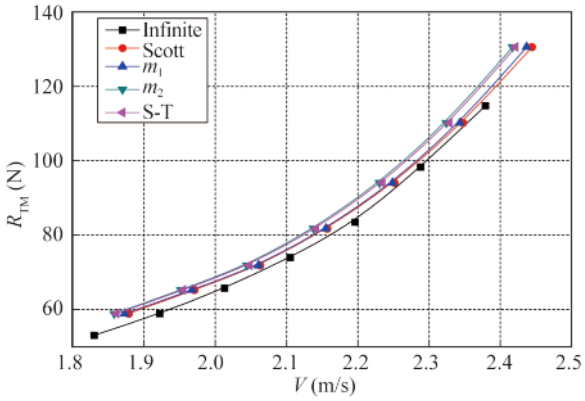

Fig. 28. Comparison of correction results for m = 2.2%.

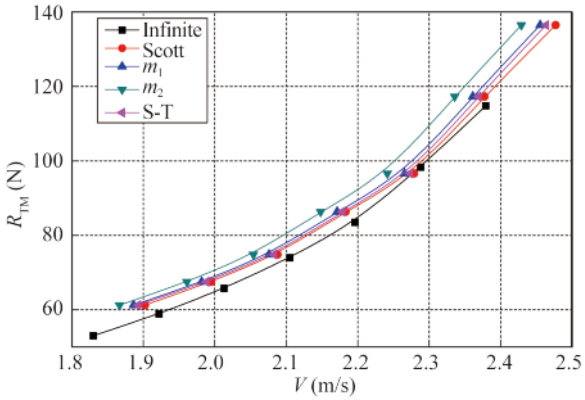

Fig. 29. Comparison of correction results for m = 3.0%.

5.2.3 *Calculation of empirical correction factor θ*

Fig. 30 shows the difference between the modified resistance curve and the resistance curve of the infinite domain. Here, Δv represents the return flow velocity calculated using the four correction formulas considered above; Δvv is the real return flow velocity in the finite domain relative to the infinite domain. Note that Δvv was measured from the velocity-resistance curve. In order to obtain a revised resistance curve that was as close as possible to resistance curve in the infinite domain, the empirical correction factor θ was defined, as shown in Eq. (8). With this approach to perform the correction, the return flow velocity calculated using a given formula is multiplied by θ to obtain the final return flow velocity.

$$\theta = \left(\frac{\Delta vv}{v}\right) \Big/ \left(\frac{\Delta v}{v}\right) = \frac{\Delta vv}{\Delta v}. \tag{8}$$

In this study, the above analysis revealed that the Scott formula has a superior correction effect to the other alternatives; however, the average flow formula is widely used because it is simple and easy to be used (Xie et al., 1978). Therefore, θ was calculated for the Scott formula and the mean flow m_1 formula; the results are presented in Table 3.

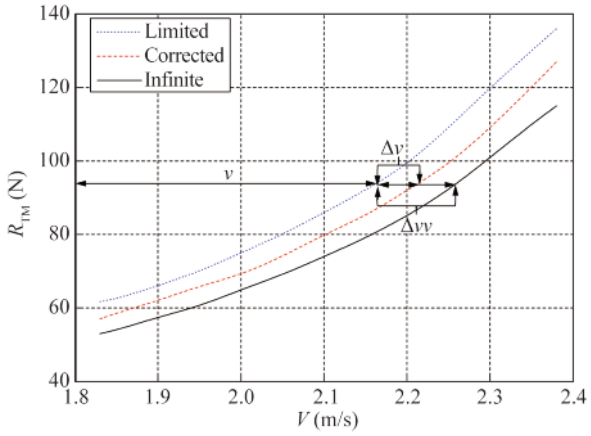

Fig. 30. Schematic diagram of return flow velocity correction.

Table 3 Empirical correction factors θ for Scott formula and mean flow m_1 formula at different blockage ratios m

Blockage ratio	1.5%		1.8%		2.2%		3.0%	
Formula	Scott	m_1	Scott	m_1	Scott	m_1	Scott	m_1
θ	0.97	0.84	1.06	1.02	1.20	1.29	1.56	1.90

When the blockage effect is actually corrected for a ship model resistance test performed in a towing tank, Δv at different speeds can be obtained according to the Scott formula or the m_1 formula. Then, according to m, θ of Δv can be obtained as shown in Fig. 31, and the final correction speed of $v' = v + \Delta v \times \theta$ can be obtained.

5.3 Experimental study of blockage effect correction method

As an experimental study of the blockage effect acting on a ship model towing tank, a resistance test was performed for the KCS model in the Harbin Engineering University towing tank. Note that the width and depth of the tank could not be adjusted according to the numerical simulation settings. Therefore, to study the blockage effect correction method, three KCS model resistance tests involving models with different λ values (Table 4) were performed in the towing tank, and the correction method proposed above was validated based on the test data.

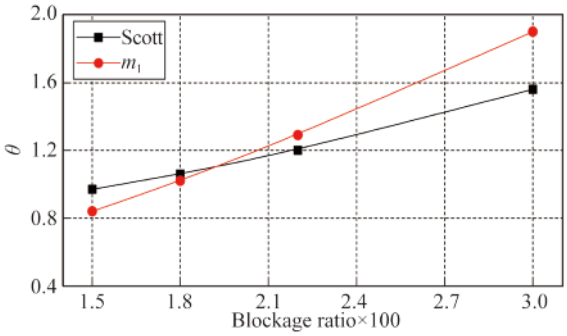

Fig. 31. Distribution of Δv correction factor θ.

5.3.1 *Experiment models*

This test was performed using the conventional ship model towing tank of Harbin Engineering University, which has dimensions of 108 m×7 m×3.5 m. The dimensions of the KCS models are given in Table 4.

5.3.2 *Comparison of wave patterns obtained for different ship model test scales*

On past experience (Sheng and Liu, 2004), the resistance components of the ship model are mainly friction, viscosity, and wave resistance. The friction resistance plays a major role when the ship speed is low, and the influence of the wave resistance is usually small. However, when ship models with different λ values were subjected to resistance testing in this study, the waves rising at the bow of the ship changed largely under small Fr.

Fig. 32 shows the bow wave patterns obtained for Ship Models 1–3 (Table 4) at Fr = 0.152. As can be seen from this figure, when the ship model is small (Ship Model 3), the wave rise caused by the ship model is consistent with that of a pressure point. However, shear waves are clearly apparent for the bow waves of Ship Models 1 and 2. The angle between the ship-traveling wave and the longitudinal profile of the ship model increases with the ship model size. This phenomenon becomes less obvious when the ship model velocity is larger (Fr = 0.282), as shown in Fig. 33. It can be seen that the wave-making conditions of the three ship models are similar to the description of the Kelvin wave system (Kim et al., 2001). Therefore, when Fr = 0.152, we believe that the main factor generating different bow waves observed for the three ship models is the ship type; that is, the scale effect. As the bulbous bow of the ship

Table 4 Main dimensions of KCS models

Parameter	Real ship	Ship Model 1	Ship Model 2	Ship Model 3
Scale ratio λ	1	31.599	37.89	52.667
Waterline length L_{WL} (m)	232.5	7.3578	6.1362	4.4145
Length between perpendiculars L_{pp} (m)	230	7.2787	6.0702	4.3671
Molded breadth B (m)	32.2	1.019	0.8498	0.6114
Molded depth D (m)	19.0	0.6013	0.5015	0.3608
Draft T (m)	10.8	0.3418	0.285	0.2051

Fig. 32. Bow wave patterns of ship models with different λ values at Fr = 0.152: (a)–(c) Models 1–3, respectively.

Fig. 33. Bow wave patterns of ship models with different λ values at Fr = 0.282: (a)–(c) Models 1–3, respectively.

model also produces a certain wave, the wave makes the pressure variation of the bulbous bow more obvious, overlapping it with the ship wave-making, and the relationship between the wave change and the ship model size is more obvious. The effect of the wave resistance on the total resistance of the ship model is small when the ship speed is low. Therefore, even though the wave patterns of ship models with different λ values are slightly variable at low speed, this has little effect on the total resistances of the ship models. Hence, it can be concluded that the differences in the total resistances of the three ship models after conversion to the behavior for a real ship are caused by the blockage effect.

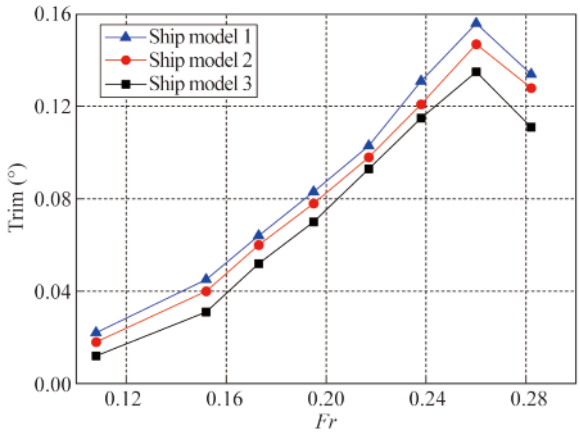

Fig. 34. Trim variations for different ship models (with different λ) as functions of speed.

5.3.3 *Comparison of ship model trims under different scale ratios*

Fig. 34 shows the ship model trim variation curves as functions of speed at different λ. As the speed increases, the value of the trimming by the bow increases gradually. When Fr exceeds 0.26, the degree of trimming by the bow decreases. The main reason is the combined effect of hydrodynamic lift and gravity. In addition, the variation trend of the ship model trim with speed is similar to that measured and calculated by Enger et al. (2010), Chen et al. (2016), Larsson et al. (2014) and others. Furthermore, as can be seen from Fig. 34, the ship models with different λ have different trim values under the same Fr. In detail, a large λ corresponds to a smaller ship model and smaller trim.

5.3.4 *Comparison of total resistances of ship models under different scale ratios*

From the above, the m values of the three ship models were 1.5%, 0.99%, and 0.51%, respectively. The resistances of the three ship models were converted to that for the real ship using the two-dimensional method and the results

were compared. The differences in resistance after conversion to the real ship case were taken have been caused by the blockage effect. Fig. 35 shows the total resistance curves of Ship Models 1–3.

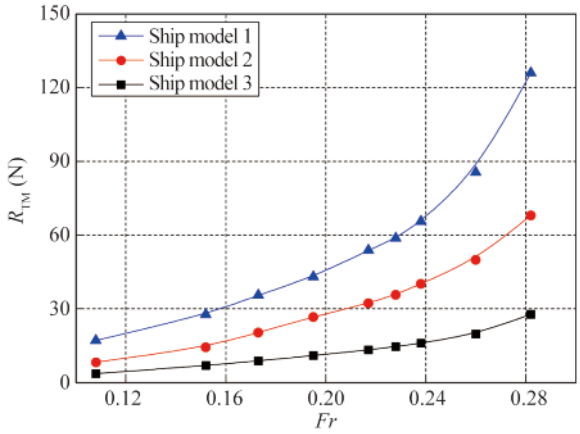

Fig. 35. Total resistance curves of ship models obtained in test.

The unmodified total resistance curves of each ship model are shown in Fig. 36. The blockage effect increased the resistance values obtained in the ship model tests, and this effect became more obvious with increases in the ship model velocity. Fig. 37 shows the corrected resistance curves of Ship Model 3 obtained using the Scott and m_1 formulas. The corrected ship resistance curves are quite close to the unmodified resistance curve and the calculated return flow velocity is very small. The total resistance curve of Ship Model 3 was selected as the resistance curve in the infinite domain. Figs. 38 and 39 show the real ship resistance curves obtained for Ship Models 1–3 corrected directly by the Scott and m_1 formulas, respectively. These figures indicate that the existence of the blockage effect increases the resistance values of the models. Furthermore, the blockage effect becomes more obvious with increased ship model velocity. In addition, the direct correction results of the Scott and m_1 formula indicate that the latter has far superior performance to the former; however, overreaction to the blockage effect is evident.

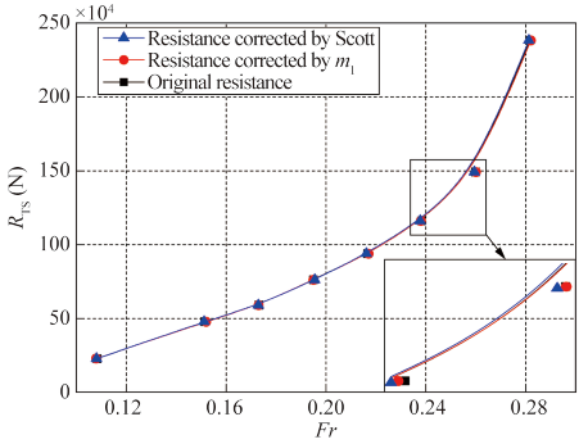

Fig. 37. Real ship resistance obtained from corrected resistance for Ship Model 3.

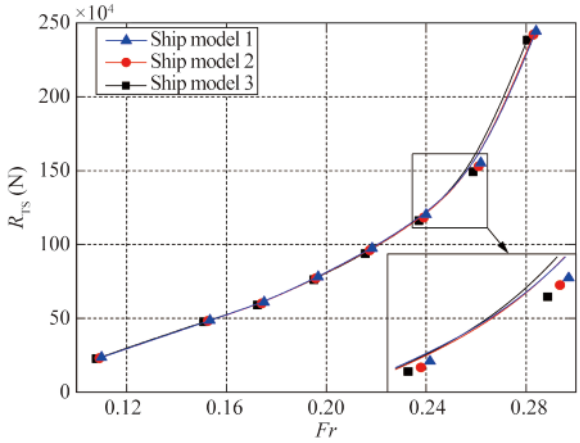

Fig. 38. Real ship resistance curves corrected by Scott formula.

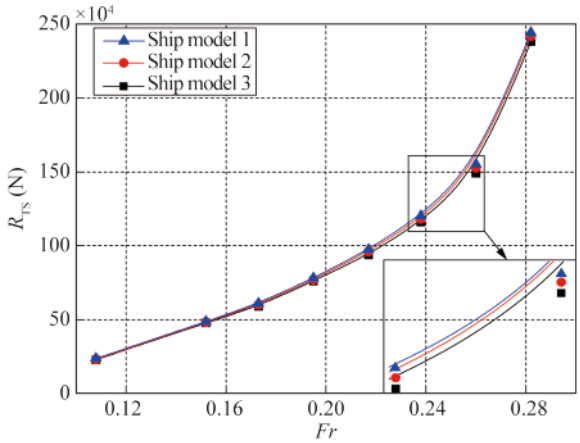

Fig. 36. Unmodified resistance curves of real ship.

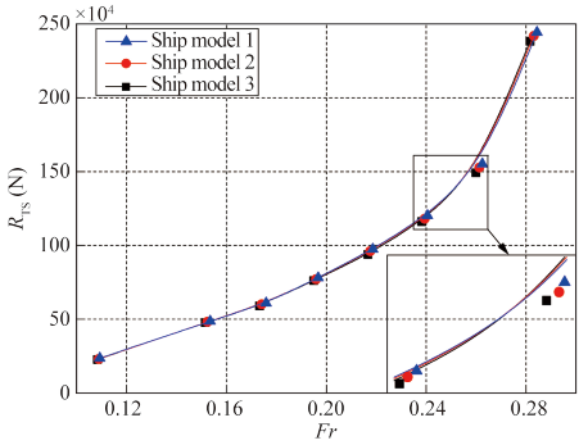

Fig. 39. Real ship resistance curves corrected by m_1 formula.

As can be seen from Figs. 38 and 39, when Fr is smaller than 0.2, the Scott and m_1 formulas can be applied directly to obtain good correction effect. When Fr exceeds 0.2, θ should be used. According to Fig. 31, for Ship Model 1, the θ values of the Scott and m_1 formulas are approximately 0.93 and 0.8, respectively; for Ship Model 2, the θ values of the Scott and m_1 formulas are approximately 0.7 and 0.6, respectively. The correction effects of the Scott and m_1 formulas are shown in Figs. 40 and 41, respectively. As the correction effect is obviously improved, use of the θ value discussed in the subsection is validated.

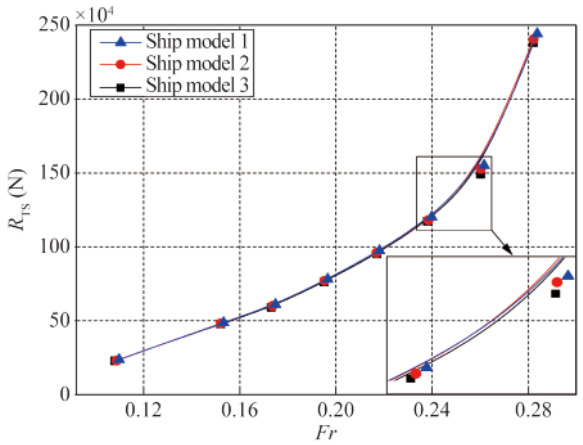

Fig. 40. Correction effect of Scott formula with empirical correction factor.

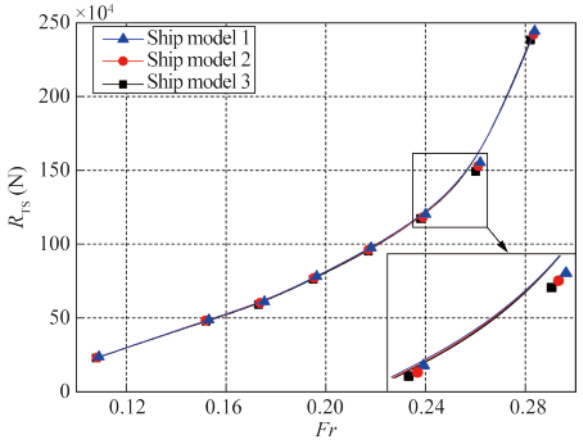

Fig. 41. Correction effect of m_1 formula with empirical correction factor.

6 Conclusions

In this study, the blockage effect mechanism and its correction were studied for the KCS. It is obvious from the comparison between the calculation and test results performed in this study that the blockage effect has a significant impact on the resistance. Therefore, when the blockage effect cannot be ignored, it is necessary to adopt appropriate correction methods. Furthermore, study of the blockage effect is of great practical significance. From the analysis performed in this study, the following conclusions were obtained.

(1) The blockage effect increases with the increase of the blockage ratio. This effect is more significant with the increase of the Froude number. Therefore, it is recommended that the blockage ratio of the ship model in a towing tank test should be smaller than 1.5%.

(2) The blockage effect causes variation of the flow velocity around the hull. The wave profile at the bow and stern becomes confused and the amplitudes of the free surface waves are increased. The blockage effect causes changes in the pressure on the bottom and side of the hull. At the stern, as a result of the velocity changes, the boundary layer separation phenomenon becomes more obvious, resulting in an unstable vortex. Hence, the bottom pressure drops significantly, resulting in increased viscous resistance. The blockage effect causes hull sinking and trimming by the stern.

(3) The blockage effect acting on the hull axial velocity distribution mainly occurs near the hull boundary layer. Under the blockage condition, the velocity increment of the bow is smaller than that of the stern. The blockage effect increases the chaotic behavior and complexity of the flow field distribution around the hull.

(4) To modify the blockage effect, the impact of the ship's parameters and blockage ratio should be considered. When the blockage ratio is smaller than 0.5%, use of the Scott or m_1 formulas for correction is recommended. When the blockage ratio is larger than 0.5% and Fr is larger than 0.2, introduction of the empirical correction factor θ to correct the resistance is recommended. For the KCS and when the blockage ratio is 1.5%, the θ values of the Scott and m_1 formulas are approximately 0.93 and 0.8, respectively. When the blockage ratio is 0.99%, the θ values of Scott and m_1 formulas are approximately 0.7 and 0.6, respectively.

References

Alderf, N., Lefrançois, E., Sergent, P. and Debaillon, P., 2010. Transition effects on ship sinkage in highly restricted waterways, *Proceedings of the Institution of Mechanical Engineers*, *Part M*: *Journal of Engineering for the Maritime Environment*, 224(2), 141–153.

Beck, R.F., 1981. Hydrodynamic forces caused by a ship in confined waters, *Journal of Engineering Mechanics Division*, 107(3), 523–546.

Chen, X., Zhu, R.C., Ma, C. and Fan, J., 2016. Computations of linear and nonlinear ship waves by higher-order boundary element method, *Ocean Engineering*, 114, 142–153.

Deng, H., Zhang, Z.H., Liu, J.B. and Gu, J.N., 2014. Nonlinear effects on hydrodynamic pressure field caused by ship moving at supercritical speed in shallow water, *Ocean Engineering*, 82, 144–149.

Enger, S., Perić, M. and Perić, R., 2010. Simulation of flow around KCS-hull, *Proceedings of the A Workshop on CFD in Ship Hydrodynamics*, Gothenburg, Sweden.

Gourlay, T., 2008. Slender-body methods for predicting ship squat, *Ocean Engineering*, 35(2), 191–200.

Gross, A. and Watanabe, K., 1972. On blockage correction, *Proceedings of the 13th ITTC*, Hamburg Berlin, Germany, pp. 209–240.

Guo, C.Y., Kan, Z., Zhao, D.G. and Wu, T.C., 2016a. Numerical study on the blockage effect of a towing tank considering ship motion, *Journal of Harbin Engineering University*, 37(12), 1619–1624. (in Chinese)

Guo, C.Y., Wu, T.C., Zhang, Q. and Gong, J., 2016b. Numerical simulation and experimental research on wake field of ships under off-design conditions, *China Ocean Engineering*, 30(5), 821–834.

Hirt, C.W. and Nichols, B.D., 1981. Volume of fluid (VOF) method for the dynamics of free boundaries, *Journal of Computational Physics*, 39(1), 201–225.

Hunt, J.C.R., Wray, A.A. and Moin, P., 1988. Eddies, streams, and convergence zones in turbulent flows, *Proceedings of the 1988 Summer Program*, Center for Turbulence Research, Stanford, pp. 193–208.

Jachowski, J., 2008. Assessment of ship squat in shallow water using CFD, *Archives of Civil and Mechanical Engineering*, 8(1), 27–36.

Kim, W.J., Van, S.H. and Kim, D.H., 2001. Measurement of flows around modern commercial ship models, *Experiments in Fluids*, 31(5), 567–578.

Larsson, L., Stern, F. and Visonneau, M., 2014. *Numerical Ship Hydrodynamics* : *An Assessment of the Gothenburg 2010 Workshop*, Springer, Netherlands.

Lataire, E., Vantorre, M. and Delefortrie, G., 2012. A prediction method for squat in restricted and unrestricted rectangular fairways, *Ocean Engineering*, 55, 71–80.

Ma, S.J., Zhou, M.G. and Zou, Z.J., 2013. Hydrodynamic interaction among hull, rudder and bank for a ship sailing along a bank in restricted waters, *Journal of Hydrodynamics*, 25(6), 809–817.

Menter, F.R., 1994. Two-equation eddy-viscosity turbulence models for engineering applications, *AIAA Journal*, 32(8), 1598–1605.

Millward, A., 1996. A review of the prediction of squat in shallow water, *Journal of Navigation*, 49(1), 77–88.

Schijf, J.B., 1949. Protection of embankments and bed in inland and maritime waters, and in overflow or weirs, *Proceedings of the 17th International Navigation Congress*, Permanent International Association of Navigation Congresses, Lisbon, Portugal, pp. 61–78.

Scott, J.R., 1970. A Comparison of four blockage correctors, *Proceedings of the 13th International Towing Tank Conference*, Volume II, Berlin.

Sheng, Z.B. and Liu, Y.Z., 2004. Watercraft principle: Ship resistance, Chapter 1, *Causes and Classification of Ship Resistance*, pp. 153–155.

Tamura, K., 1975. "Blockage correction" proceedings, *Proceedings of 14th International Towing Tank Conference*, Volume III, Ottawa.

Wang, X.G., Zou, Z.J., Yu, L. and Cai, W., 2015. System identification modeling of ship manoeuvring motion in 4 degrees of freedom based on support vector machines, *China Ocean Engineering*, 29(4), 519–534.

Wilcox, D.C., 1998. *Turbulence modeling for CFD*, United States of America by Griffin Printing, Glendale, California, pp. 84–87.

William Jr., H. and Pope, A.R., 1984. *Low-Speed Wind Tunnel Testing*, second ed., Wiley, New York, pp. 133–135.

Wu, B.S., 2007. On geometric parameters in uncertainty analysis of measurement in ship model test, *Journal of Ship Mechanics*, 11(3), 363–372.

Xie, K.Z., Zhou, Z.Q., Song, J.J., Shen, H.Y. and Ye, B.J., 1978. The experiment study of blockage effect of the tank, *Journal of Shanghai Ship and Shipping Research Institute*, 1(2), 1–27. (in Chinese)

Yao, Z.Q., Shen, H.C. and Gao, H., 2013. A new methodology for the CFD uncertainty analysis, *Journal of Hydrodynamics*, 25(1), 131–147.

Zaghi, S., Muscari, R. and Di Mascio, A., 2016. Assessment of blockage effects in wind tunnel testing of wind turbines, *Journal of Wind Engineering and Industrial Aerodynamics*, 154, 1–9.

Zhang, Z.H., Deng, H. and Wang, C., 2015. Analytical models of hydrodynamic pressure field causing by a moving ship in restricted waterways, *Ocean Engineering*, 108, 563–570.

Zhou, G.L., 2002. *Uncertainty Analysis of Ship Model Towing Resistance Experiment*, MSc. Thesis, Harbin Engineering University, Harbin. (in Chinese)

Zhou, M.G., Zou, Z.J. and Yao, J.X., 2013. Prediction of ship squat in restricted waters, *Journal of Ship Mechanics*, 17(6), 625–634. (in Chinese)

Zou, L. and Larsson, L., 2013a. Numerical predictions of ship-to-ship interaction in shallow water, *Ocean Engineering*, 72, 386–402.

Zou, L. and Larsson, L., 2013b. Computational fluid dynamics (CFD) prediction of bank effects including verification and validation, *Journal of Marine Science and Technology*, 18(3), 310–323.